THE ASTROPHYSICAL JOURNAL, Vol 152, April 1968

THE X-RAY EMISSION SPECTRUM OF A SOLAR ACTIVE REGION

K. EVANS AND K. A. POUNDS*
Department of Physics, University of Leicester, England
Received September 12, 1967; revised October 19, 1967

ABSTRACT

Absolute intensities are presented for twenty-eight identified and four unidentified solar X-ray emission lines between 11 and 22 Å measured during a Skylark rocket flight on May 5, 1966 It is found that the total line emission exceeds the X-ray continuum by at least a factor of 5, and this is shown to be consistent with an emission model derived from the observed line spectra. Excellent agreement is found between the total flux and a simultaneous observation obtained with a broad-band (8–20 Å) ion chamber of the NRL SOLRAD satellite series. Of the measured emission lines, those of O VII are distinct, both in their observed profiles and in consideration of the coronal temperatures at which they are efficiently produced. These lines are interpreted as arising principally from the general coronal disk at a temperature between 10^6 and 1.5×10^6 ° K. In contrast, all the other observed lines show a strong component clearly associated with a coronal active region, and the absolute line intensities are used here to derive a model of this region Good agreement of the calculated and observed spectra of O VIII, neon, iron, and nickel is obtained with the bulk of the active region plasma at a temperature of 3×10^6 ° K The corresponding value of $N_e^2V = 1\,7 \times 10^{48}$ cm^{-3} is consistent both with the non-observation of a solar continuum below 14 Å and with the separate values of N_e^2 and V obtained for similar active regions from recent broad-band X-ray photographs Element abundances for neon, iron, and nickel are determined relative to oxygen and are found to be in good general agreement with values obtained from analyses of solar ultraviolet spectra.

I. INTRODUCTION

Two slitless Bragg spectrometers were successfully flown on a sun-pointed Skylark rocket (SL 304) from Woomera, South Australia, on May 5, 1966, to measure the solar X-ray emission below 25 Å. The rocket launch took place at 04.14 hours (U.T.) during a relatively quiet period of solar activity. In particular, no solar flares have been reported in a period of several hours around the launch time. Several weak plages and decimeter radio emission regions were visible on the solar disk, contributing to a 10.7-cm index of 90. A contour map (Fig. 1) produced from the 9.1-cm heliograph data of Stanford University Observatory shows the sources of excess radio emission across the northern hemisphere of the Sun on May 4. It may be seen that the dominant active center lies near the northwest limb and is apparently associated with plages 8278 and 8279. Recent solar X-ray photographs (e.g., Pounds and Russell 1966) have shown that such regions invariably appear as bright X-ray sources, and indicate local densities up to an order of magnitude higher than the normal corona. Further, the increasing contrast of these local X-ray emission regions to the coronal disk itself, evident for wavelengths below 20 Å, has been interpreted as showing that the "coronal condensations" are also hotter than the general coronal material. The analysis of visible emission lines from a coronal condensation (e.g., Letfus 1965) supports this conclusion.

A brief account of the flight of Skylark 304 and the identification of the observed solar emission lines has been reported previously (Evans, Pounds, and Culhane 1967). The spectrum includes a number of important, high-temperature emission lines of Ne IX and X, Fe XVII and XVIII, and Ni XIX that had not previously been seen on the Sun. Table 1 of the present paper lists these emission lines and gives their absolute intensity at Earth's distance during the May 5 flight. A tentative identification of the line at 13.65 Å, as a satellite of Ne IX (Sawyer, Jahoda, Ribe, and Stratton 1962) is suggested,

* Part of the analysis reported here was carried out when one author (K A. P) was a Visiting Scientist at American Science and Engineering, Cambridge, Massachusetts.

TABLE 1

SOLAR X-RAY SPECTRUM OF MAY 5, 1966*

Ion	Transition	Wavelength (Å)	Recorded Counts 1	Recorded Counts 2	Detector Efficiency (per cent)	Crystal Reflection Coefficient (10^{-5} radian)	Line Intensity (10^{-5} erg cm^{-2} sec^{-1}) 1	Line Intensity (10^{-5} erg cm^{-2} sec^{-1}) 2	f-Values†
O VII	$1s^2\ ^1S_0$–$1s2p\ ^1P_1$	21.60	16.1		0.2	1.75	363		0.69 (*a*)
	$1s3p\ ^1P_1$	18.63	18.9		2.1	2.40	56		0.15 (*a*)
	$1s4p\ ^1P_1$	17 77	10.9		3.5	2.65	18		0 07
	$1s2p\ ^3P_1$	21.80	7 7		0.2	1.70	193		
O VIII	$1s\ ^2S_{1/2}$–$2p\ ^2P_{1/2,3/2}$	18.97	45.5	15.1	1.5	2.3	130	54	0.42
	$3p\ ^2P_{1/2,3/2}$	16.01	28.7	14.8	7.5	3.3	20	10	0.08
	$4p\ ^2P_{1/2,3/2}$	15.17	24	14	9 7	3.55	12	7	0.03
	$5p\ ^2P_{1/2,3/2}$	14.82	4.9		10.8	3.65	2.2		0.01
Ne IX	$1s^2\ ^1S_0$–$1s2p\ ^1P_1$	13.45	60	26	17.3	4.5	18	7.8	0.72 (*a*)
	$1s3p\ ^1P_1$	11.56	17.5	8.1	31.8	6.65	2.3	1.0	0.15 (*a*)
	$1s2p\ ^3P_1$	13.55	24	12.5	16.7	4.4	7 4	3.9	
Ne X	$1s\ ^2S_{1/2}$–$2p\ ^2P_{1/2,3/2}$	12.13	28	12	26.8	5.9	1.7	(0.7)	0.42
Fe XVII	$1s^22s^22p^6\ ^1S_0$–$1s^22s^22p^53s\ ^3P_1$	17.05	76	29	4.9	2.85	84	32	0.11 (*b*)
	$1s^22s^22p^53s\ ^1P_1$	16.77	34	14	5.6	2.95	32	13	0.10 (*b*)
	$1s^22s^22p^53d\ ^3P_1$	15.45	39.2	18.2	8.8	3 4	22	10	0.01 (*b*)
	$1s^22s^22p^53d\ ^3D_1$	15.26	91	35	9.3	3.5	48	18.5	0.64 (*b*)
	$1s^22s^22p^53d\ ^1P_1$	15.01	151	56	10.4	3.6	74	27.5	2.24 (*b*)
	$1s^22s^22p^63p\ ^1P_1$	13.82	25	9.6	15.1	4.2	8.8	3.2	
	$1s^22s^22p^54d\ ^3D_1$	12.26	19.8	8.2	25.9	5.8	2.5	1.2	0.37 (*c*)
	$1s^22s^22p^54d\ ^1P_1$	12.12	(blends with Ne X)		26.8	5.9	2.8	(1.2)	0.41 (*c*)
Fe XVIII	$1s^22s^22p^5\ ^2P_{3/2}^o$–$1s^22s^22p^4(^3P)3d\ ^2D_{5/2}$	14.40	7.0		12.4	3.9	4.5		1.90 (*d*)
	$1s^22s^22p^4(^1D)3d\ ^2D_{5/2}$	14.25	11.2		13.0	4.0	2.7		3.11 (*d*)

* The recorded counts in each line are the average of the four scans and are listed as main and secondary components under 1 and 2, respectively. The detector efficiency and crystal reflection coefficient used in converting from counts to the line intensities in the final column are shown for each wavelength. For the broad O VII lines and for the weakest lines, only one component is given. The division of the 12.13 Å flux into Ne X and Fe XVII components has been made by calculating the intensity of Fe XVII 12.12 Å from the observed Fe XVII 12.26 Å intensity using the relative *f*-values for these two $2p$–$4d$ lines.

† (*a*) W. L. Wiese, M. W. Smith, and B. M. Glennon, *Atomic Transition Probabilities*, Vol. 1, *H to Ne* (NBS Reference Data Series, 1966). (*b*) C. Froese, *B.A.N.*, 19, 86 (1967). (*c*) C. Froese-Fischer, private communication (1967). (*d*) S. Kastner and J. H. Underwood, private communication (1967).

TABLE 1—*Continued*

Ion	Transition	Wavelength (Å)	Recorded Counts		Detector Efficiency (per cent)	Crystal Reflection Coefficient (10^{-5} radian)	Line Intensity (10^{-5} erg cm^{-2} sec^{-1})		f-Values†
			1	2			1	2	
Ni XIX.	$1s^22s^22p^6\ ^1S_0$–$1s^22s^22p^53s\ ^3P_1$	14.03	8.5	4.2	14.0	4.1	2.9	1.5	0.08 (*d*)
	$1s^22s^22p^53s\ ^1P_1$	13 77	18	8.4	15.5	4.3	5.8	2.8	0 06 (*d*)
	$1s^22s^22p^53d\ ^3P^1$	12.80	9 0	3.5	21.5	5.1	2.3	1.0	0.01 (*d*)
	$1s^22s^22p^53d\ ^3D_1$	12.64	12.5	4.8	22.6	5.3	3.1	1.2	0.92 (*d*)
	$1s^22s^22p^53d\ ^1P_1$	12.24	18.0	6.9	24.6	5 6	3.6	1.5	2.43 (*d*)
Unidentified lines:									
.. ..	... . .	12.53	13.9	5.5	23.5	5 45	3.1	1.3	.
Possibly Ne VIII.	$1s^22s$–$1s2p2s$	13 65	9		16.0	4.35	3		.
..	. . .	16.3	5.6		6.7	3.1	4.4		.
..... .	. ...	16.6	10.6		6.0	3.0	9		.

though no detailed study of the probability of occurrence of this line in the low density coronal plasma has been made.

II. FLIGHT RESULTS AND SPECTRAL ANALYSIS

In the flight of Skylark 304, solar pointing was achieved approximately 100 sec after launch and maintained until re-entry 274 sec later. Rocket apogee was 181 km, and the atmospheric attenuation, for the X-ray wavelengths being measured, was small throughout most of the controlled flight. Both spectrometers had plane crystals of potassium acid phthallate (KAP), with lattice constant = 13.30 Å, and pillbox proportional counters, selected for their low background counting and the ability to discriminate against higher orders. A general description of the properties of the pillbox type of

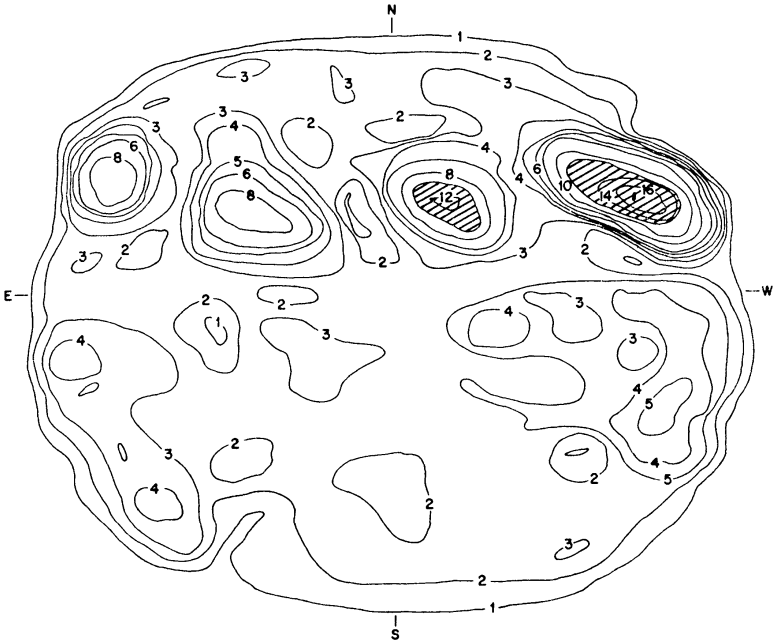

FIG 1 —9 1-cm radioheliograph of 21^h U T , May 4, 1966, produced from pencil-beam observations made at Stanford University Observatory. Contours represent radio brightness temperatures in units of 10^4 ° K The two bright sources in the northwest quadrant of the solar disk contain 68 per cent of the total active region component radio flux and are associated with the two moderate sized plages (Nos. 8279 and 8284) present on the visible solar disk.

proportional counter has been published elsewhere (Culhane, Herring, Sanford, Phillips, and O'Shea 1966). For the present flight counters, the mean conversion gain was 3×10^{-13} coulomb/keV, with a strictly linear multiplication factor and a measured energy resolution given by $\sigma = 0.22\ E^{-0.5}$, where σ is the standard deviation of the output pulse distribution for photons of energy E(keV). The detector efficiency for each measured emission line was computed from the detector characteristics (window of 0.52 mg/cm² Melinex, coated with 1.08×10^{-2} mg/cm² aluminum; gas filling to 1.27 cm atm of 90:10 argon-methane), using known absorption coefficients. The efficiency at each particular wavelength is given in the fifth column of Table 1.

Considerable effort was expended to limit the "background" count rate in flight, particularly in the hope of measuring the solar X-ray continuum, which the only previous flight (Blake, Chubb, Friedman, and Unzicker 1965) had indicated to be weak. Thus a combination of low-noise amplifier, energy-resolving detector, and pulse-height selection was chosen. The selector accepted only those pulses corresponding to an input

to the detector between 0.33 and 1.2 keV. Effectively all electronic noise pulses and any pulses arising from solar ultraviolet photons being transmitted by the (high-opacity) detector window fell below the lower threshold and were not counted. The detector pulses arising from cosmic-ray-induced events in the rocket structure and the instrument itself were largely rejected by choosing the detector gas filling so that the mean energy deposition was considerably above 1.2 keV. The success of this background rejection system is indicated by the low count rates obtained in flight, between the individual emission lines. At the extremes of each spectral scan, a small correction was necessary to account for the photon pulses in one wing of the detector distribution being rejected by the pulse-height selector. In practice, only the O VII 21.6 Å line was significantly affected, and here the correction factor was only 8 per cent.

Absolute wavelength calibration of the spectrometers was obtained by means of a standard metrological calibration of the shaft encoder to set the Bragg angle read-out scale. The absolute photon sensitivity of the instrument required measurement of the KAP crystal reflection coefficient as a function of wavelength. This was achieved by the method of James (1948), with the modification of using a proportional counter for the original ion chamber. Two separate laboratory instruments were employed—the reflectometer described by Underwood and Stewardson (1966), and a single-crystal spectrometer with characteristic line source and Soller collimation, described briefly by Charles and Cooke (1967). The integrated reflection coefficient was measured for a number of wavelengths and found to be consistent with previous measurements (e.g., Blake 1966) to about 30 per cent, the present values being consistently lower by this amount.

Four spectral scans, over the wave band 11–25 Å, were obtained during the flight, and the averaged count rate versus wavelength record is shown in Figure 2. Table 1 lists the mean photon count in each spectral line (being the average of all four scans), the detector and crystal efficiencies, and the computed absolute line intensities. Though small interscan variations were observed in several lines, these were within the expected statistical distribution. Hence, only the mean counts per line have been used to compute each line intensity. Thus, for a mean total count of N_λ above background at wavelength λ (Å), the line intensity E_λ is given by

$$E_\lambda(\text{ergs cm}^{-2}\text{ sec}^{-1}) = \frac{2 \times 10^{-8} N_\lambda \omega}{T_{\lambda,h} A_\lambda R_\lambda P_\lambda \lambda}, \quad (1)$$

where ω is the scanning rate in radians per second and R_λ and P_λ are the crystal reflection coefficient (radians) and detector efficiency for photons of wavelength λ, respectively. The atmospheric attenuation, a function of the altitude (h) of each individual spectral scan, and ranging between zero and 30 per cent, is represented by $T_{\lambda,h}$. The effective crystal area (A_λ) also varies with the angle of incidence to the crystal and, hence, with λ and is 1 cm^2 at normal incidence.

For many of the emission lines two intensities are listed in Table 1. This is a consequence of the manner of operation of a slitless, scanning spectrometer. For any monochromatic emission the crystal will reflect efficiently over a narrow range of angles, corresponding to the width of the main diffraction maximum of the crystal, and this width increases over the wavelengths covered from about 4′ at 11 Å to 11′ near 22 Å. The observed line profile is a folded integral of this diffraction property and the source function. The recent solar X-ray photographs, referred to earlier, show a measurable X-ray emission from the whole solar disk. They also show that the emission below 20 Å comes principally from active centers which are, typically, only 1′ or so in diameter (e.g., Pounds and Russell 1966; Reidy, Vaiana, Zehnpfennig, and Giacconi 1968). Two points follow: First, it is vital to scan the spectrometer smoothly, so that a proper integration of the smallest source is obtained; second, a complete line profile may extend to

over 30′ in effective width. In the current experiment an essentially continuous scan was used, and the results show line profiles of two distinct types. The O VII lines were each smooth and broad, being emitted apparently from the whole solar disk. All other line profiles had a more complex structure with a dominant emission peak centered about 10′ or 0.07 Å to the short wavelength side of the predicted value, and apparently originating in the dominant northwest activity region.

The analysis was complicated in some parts of the spectrum by the overlapping of the profiles of adjacent emission lines. Two such spectral regions, near 15 and 17 Å, and the method of analysis of each profile into a main and a secondary peak, are illustrated in Figure 3. The main active region component of each line is listed in Table 1 and shown in Figure 4, separately from the remaining emission. It is suggested in the discussion in the second half of this paper that the secondary component of each line, with the exception of the O VII series, is associated with the weaker plages extending across the northern hemisphere on to the eastern side of the Sun and that very little emission in the observed lines of neon, iron, nickel, and O VIII comes from the general coronal disk.

The counting rate between the discrete emission lines was low throughout the spec-

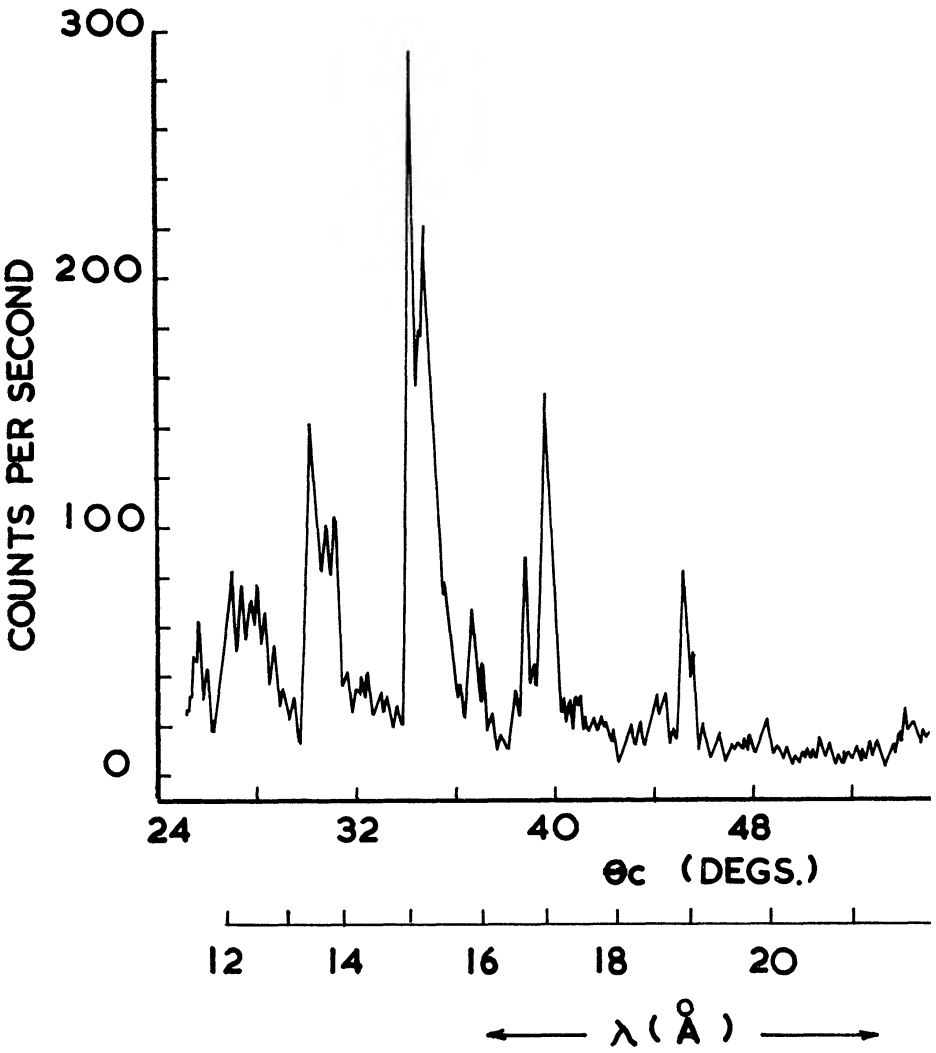

FIG. 2.—Flight data averaged over the four spectral scans

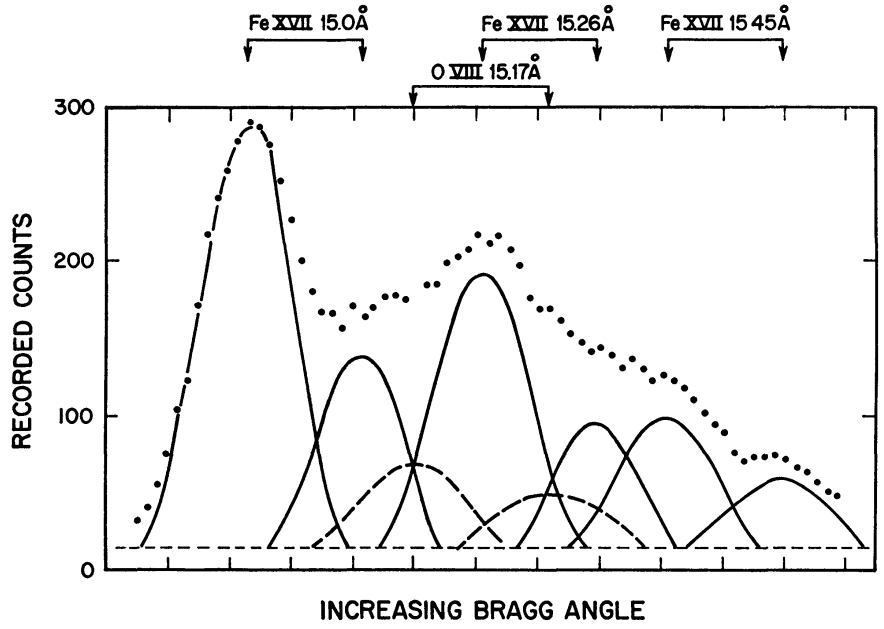

FIG. 3*a*

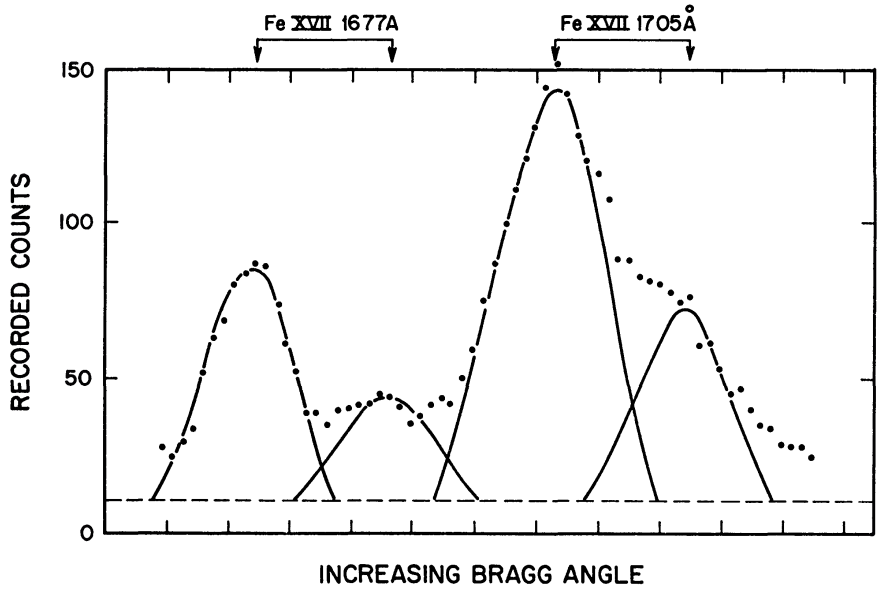

FIG 3*b*

FIG. 3.—(*a*) A complex emission line group near 15 Å is resolved into three double-component lines of Fe XVII. The unfolding of this group has been achieved by first completing the stronger component of the 15.0 Å line above the background counts (*dashed line*) and next adding the strong components at 15.26 and 15.45 Å, in the knowledge that each instrumentally broadened profile is symmetrical and of essentially equal width. Finally, each weaker component has been added, with common width, equal relative area to the main peak and angular separation from the main peak. The same two-component profile has been used for all the observed Fe XVII lines (cf. Fig. 3*b*). The dashed profiles represent an approximate upper limit for O VIII Lyman-γ. (*b*) A simpler emission line group near 17 Å is resolved into two-component profiles of two Fe XVII lines. Here, as in Fig. 3*a*, the main components are found to lie about 10′ to the low Bragg angle side of the predicted position, consistent with an emission center in the western hemisphere of the Sun.

tral scan, rising only slowly from about 7 counts per second near 20Å to 15 cps at 11.5 Å. In addition, no significant increase is seen to the short wavelength side of 16.8 or 14.2 Å (the recombination limits of O VIII and O IX). Evidently, the solar continuum radiation is quite weak compared with the observed line emission, a result at marked variance with one recently reported from a similar study conducted by the NRL group (Fritz, Kreplin, Meekins, Unzicker, and Friedman 1967), but in general agreement with the observations of Rugge and Walker (1967). An upper limit to the continuum is obtained in the present case by taking the over-all particle count rate equal to the long wavelength background reading of 7 cps. At this end of the spectrum, the window absorption and near-normal incidence of the crystal militate strongly against X-ray counts from either a true solar continuum or X-radiation scattered from the crystal. Thus, if *all* the additional background counts toward shorter wavelengths are solar continuum, the following upper limits are obtained:

$$\text{Total continuum (11–20 Å)} \leq 1.5 \times 10^{-3} \text{ erg cm}^{-2} \text{ sec}^{-1},$$

$$\text{Continuum-to-line ratio (11–20 Å)} \leq 0.20,$$

$$\text{Continuum below 14.25 Å} \leq 2.8 \times 10^{-4} \text{ erg cm}^{-2} \text{ sec}^{-1},$$

$$\text{Continuum-to-line ratio (11–14.25 Å)} \leq 0.26.$$

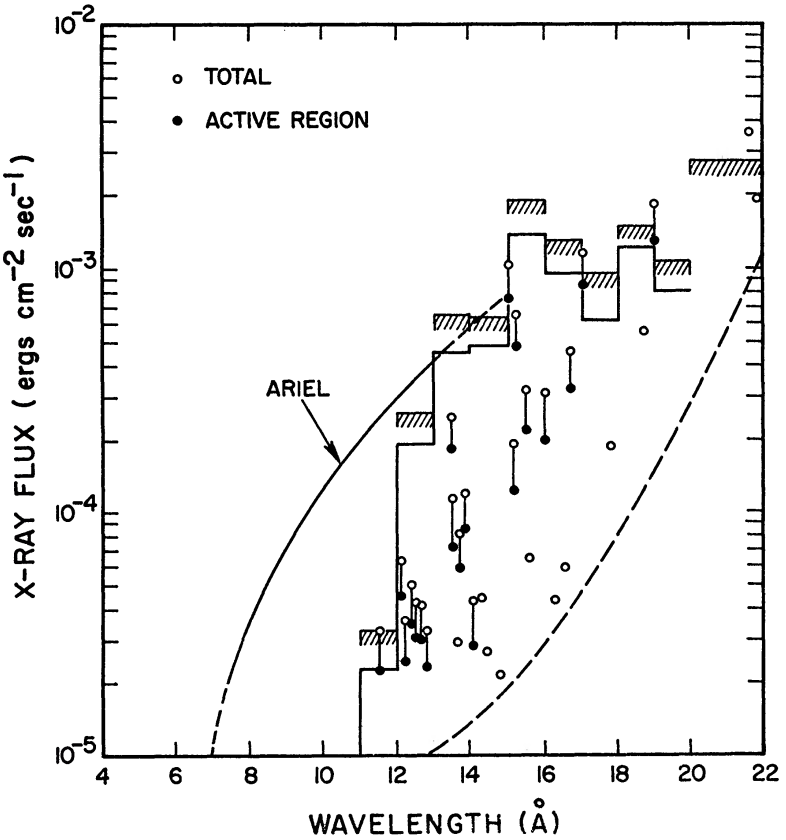

FIG. 4.—Absolute intensity of each emission line listed in Table 1 is plotted and the total flux summed in Å bands, separately for the strong active region components and for the total line emission. Also shown is a low-resolution spectrum obtained from the Ariel 1 satellite proportional counter spectrometer under similar solar activity conditions (no flares, 10-cm index = 96). The dashed line has been included to illustrate the steeply rising sensitivity threshold at longer wavelengths, resulting mainly from the decreasing detector efficiency. The ordinate flux units are per angstrom for the histograms and Ariel spectrum and per line otherwise.

The precision of the absolute line intensities is primarily statistical for the weak lines, while increasing sensitivity to detector efficiency will also add to the errors toward the longer wavelengths. An assessment of all the possible sources of error indicates that the measured absolute strength of all but the weakest lines should be correct to better than a factor 2 below 17 Å and a factor 4 at 22 Å. Furthermore, the relative intensities of lines should be considerably more precise. An important example is the O VIII Ly-α and Ly-β lines, at 19 and 16 Å, respectively, for which the measured intensity ratio should be accurate to better than 20 per cent. For the shorter wavelengths, the interline ratios should be accurate to better than 10 per cent, except where considerable blending with a stronger line is involved.

Some confirmation of the estimated errors in the absolute flux values may be derived from a comparison of the integrated flux in the present spectrum with an ion-chamber measurement obtained from the U.S. Naval Research Laboratory's SOLRAD satellite. The May 5 satellite data, kindly supplied to the authors by Dr. R. W. Kreplin of NRL, show several values obtained within a few hours of the present rocket flight, and only small variations are apparent, consistent with the absence of flares and with only weak plages activity. A typical value, obtained shortly before the rocket launch is expressed by NRL as

$$\text{Total intensity (8–20 Å)} = 2.8 \times 10^{-3} \text{ erg cm}^{-2} \text{ sec}^{-1} .$$

In comparison, a summation of all lines in the present spectrum (Fig. 4) gives

$$\text{Total line intensity (11–20 Å)} = 7.4 \times 10^{-3} \text{ erg cm}^{-2} \text{ sec}^{-1} .$$

To this may be added

$$\text{Total intensity in best-fit Ariel spectrum (10.7-cm index = 96)}$$
$$\text{(8–11 Å)} = 0.5 \times 10^{-3} \text{ erg cm}^{-2} \text{ sec}^{-1},$$
$$\text{Upper-limit continuum (11–20 Å)} = 1.5 \times 10^{-3} \text{ erg cm}^{-2} \text{ sec}^{-1},$$
$$\text{total} = 9.4 \times 10^{-3} \text{ erg cm}^{-2} \text{ sec}^{-1} .$$

The agreement is apparently on the limit of the estimated errors in the absolute intensities from the present experiment. However, the NRL ion-chamber output is conventionally analyzed with an assumed 2×10^6 ° K gray-body spectrum. If the *actual* spectral shape of Figure 4 is used instead, the NRL figure becomes

$$\text{Total intensity (8–20 Å)} = 9.2 \times 10^{-3} \text{ erg cm}^{-2} \text{ sec}^{-1} .$$

The agreement may now be considered excellent, considering the two quite different techniques involved, and is within the spread of values given for the ion-chamber experiment.

III. DISCUSSION

High-resolution spectra of the type reported here are of particular value in providing the most direct evidence of the physical parameters of a coronal active region. In comparison, interpretation of radio data may be confused by a contribution from the chromosphere and, where strong magnetic fields are present, by gyroradiation, while the observation of visible emission lines is restricted to the solar limb and involves long line-of-sight integration through the corona.

For a quantitative assessment of the May 5 spectrum, it is assumed that each emission line results from the population of the lower excited states of an ion by electron collision from the ground state. The neglect of recombination from a higher stage of ionization,

followed by cascade into the lower excited levels, should be relatively unimportant for the strong resonance lines of the present spectrum. Thus, each collisional excitation to an excited state is followed by the emission of one photon of corresponding energy, and the intensity of the resulting emission line measured above Earth's atmosphere may be expressed (e.g., Pottasch 1964) as

$$E(\text{ergs cm}^{-2}\text{ sec}^{-1}) = 8 \times 10^{-43} \bar{g} f A_z \int G(T_e) N_e^2 dV \,. \quad (2)$$

Here A_z is the coronal abundance of the particular element relative to hydrogen, $\bar{g}$ is the average Gaunt factor and is taken equal to 0.3 for each case considered, and f is the oscillator strength between the ground level and the particular excited state. The f-values assumed here are given in the last column of Table 1. The function $G(T_e)$ relates

TABLE 2

FRACTIONAL ABUNDANCE OF THE IONS REPRESENTED IN THE PRESENT SPECTRUM*

Ion	Electron Temperature (10^6 °K)									
	1	2	3	4	5	6	7	8	9	10
O VII	1 00	0 56	0 13	0 02	0 007	0 003	0 001	. . .	. . .	.
O VIII	0 007	.36	.34	17	08	05	.03	0 02	0 01	. . .
O IX	. . .	08	.53	.81	91	.95	97	98	.99	1 00
Ne IX	0 87	97	81	.52	34	12	05	03	02	0 01
Ne X		.02	17	37	.40	32	23	16	.11	0 09
Ne XI	.	....	01	10	25	55	71	81	87	0 90
Fe XVII	.	015	31	50	58	58	54	46	38	0 28
Fe XVIII		....	.005	03	08	.14	21	27	29	0 29
Ni XIX	..	001	10	24	35	44	48	48	44	0 40
Fe XVII	. .	0 030	0 31	0 44	0 46	0 46	0 43	0 37	0 30	0 22

*O VII–Fe XVIII data from J. W. Allen and A K Dupree (1967), *Harvard College Obs Report*, No 24; Fe XVII and Ni XIX data from C Jordan (unpublished).

the efficiency of producing a given emission line to the electron temperature (T_e) and is given by

$$G(T_e) = T_e^{-0.5} \times 10^{-5040W/T_e} A_{zi} \,,$$

where W is the excitation potential (in eV) of the state concerned and A_{zi} is the fraction of element Z in the ith state of ionization. Computed values of the ionization distributions of oxygen, neon, iron, and nickel are listed in Table 2, and the resulting $G(T_e)$ functions for several lines in the present spectrum are shown in Figures 5–8. The ionization distributions have been calculated by Allen and Dupree (1967) and by Jordan, as referenced, taking into account collisional ionization, auto-ionization, radiative recombination, and dielectronic recombination. The corresponding rate coefficients are each functions of electron temperature, and the resulting ionization equilibria are strongly temperature-dependent. This is a most important factor in assessing the present solar X-ray spectrum. Thus, it is evident from Table 2 that only O VII, of the ions represented in the spectrum, is likely to exist in a significant abundance in the general corona (for which a temperature of 10^6 to 1.5×10^6 ° K may be assumed), in agreement with the observed, unique width of the O VII line profiles. Apparently a significantly higher temperature must be found in the active regions to give the observed strong emission of the neon, iron, nickel, and O VIII lines.

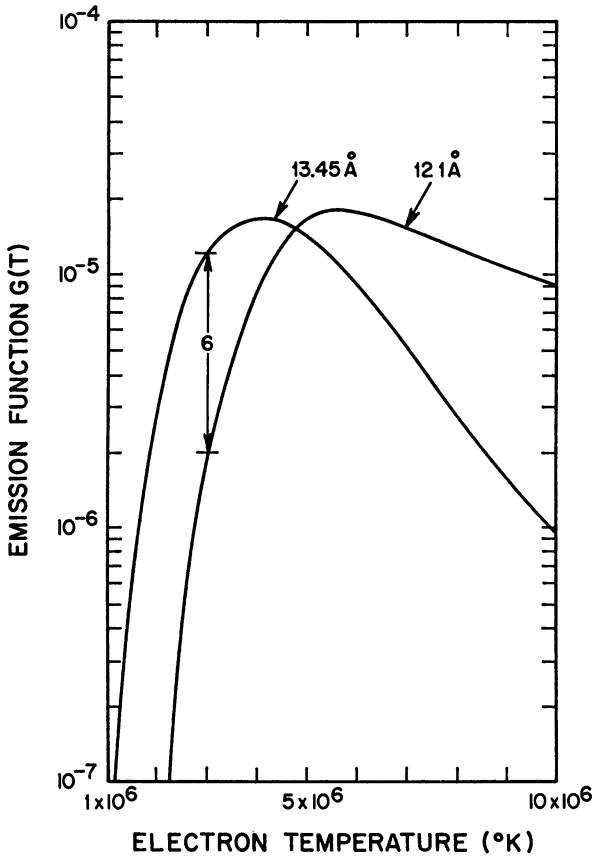

FIG. 5 —Emission function $G(T_e)$ for the first principal series line of Ne IX and for Ne X Lyman-α The intensity ratio of these lines is shown in the text to require a $G(T_e)$ ratio of 6, indicating a source electron temperature close to 3×10^6 ° K. Note that the ordinate is wrongly labeled $G(T)$; it should have been labeled $G(T_e)$.

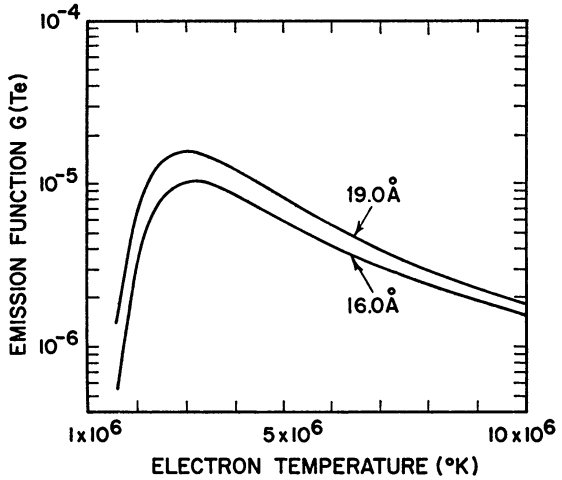

FIG. 6.—Emission functions computed for the O VIII Ly-α and Ly-β lines

a) Active Region Temperature

For a first analysis, it is assumed that all the active region material is at a single temperature, a situation that may be grossly realized and that can be tested later. Now, for an active region temperature T, the intensity of the corresponding main component of any emission line is given by

$$E = 2.4 \times 10^{-43} f A_z G(T) N_e^2 V \,, \tag{3}$$

where $N_e^2 V$ now represents the effective "size" of the active region. The value of T for the emitting region may now be obtained by comparing the observed intensity of any pair of lines. To avoid errors in the published element abundances, lines of the same element are preferred. Thus, a comparison of Ne IX 13.45 Å and Ne X 12.1 Å gives, using equation (3) and with f-values from Table 1,

$$\frac{G(T)_{13.4\text{Å}}}{G(T)_{12.1\text{Å}}} = \frac{18 \times 10^{-5}}{1.7 \times 10^{-5}} \left(\frac{0.42}{0.72}\right) \simeq 6 \,.$$

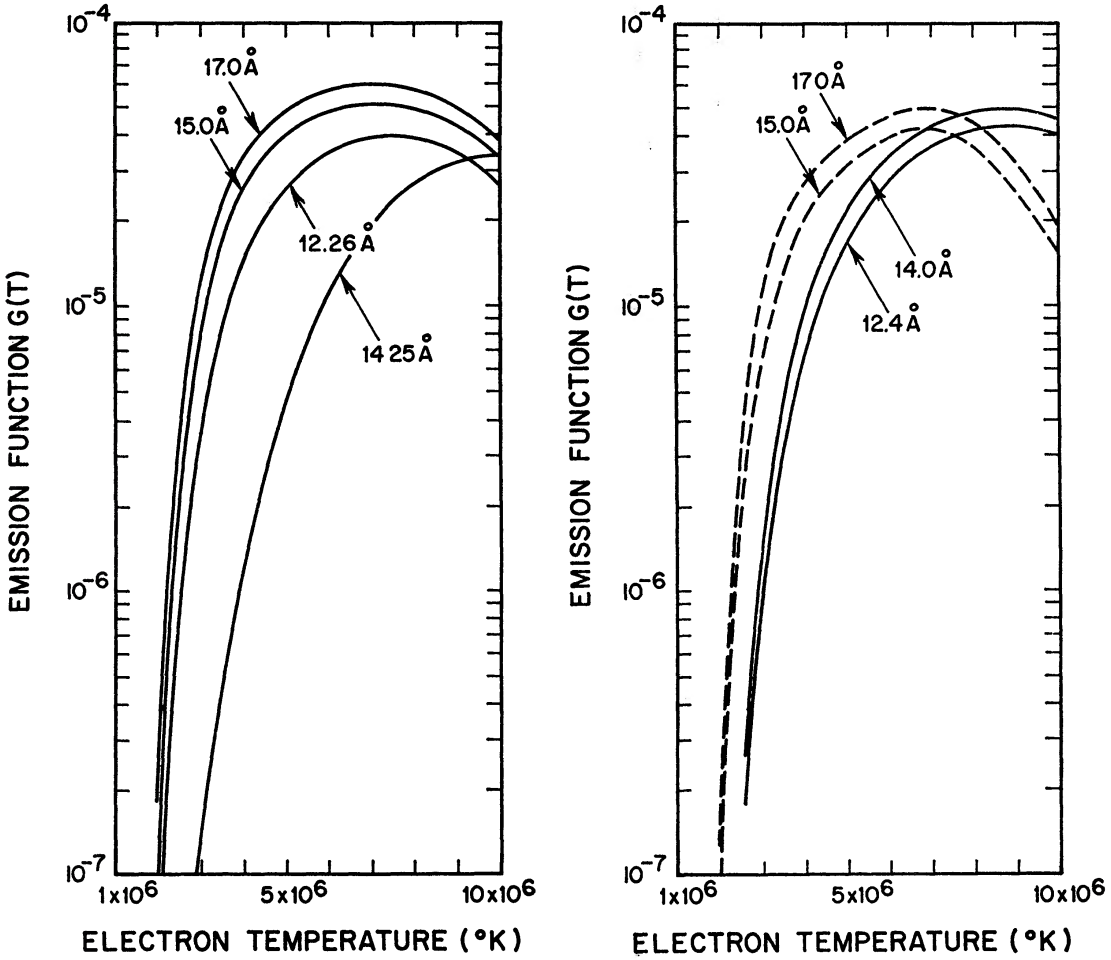

FIG. 7 (*left*).—Emission functions computed for three emission lines of Fe XVII and for Fe 14.25 Å.

FIG. 8 (*right*).—Emission functions for two lines of the isoelectronic series of Fe XVII (*dashed curves*) and Ni XIX (*full curves*). For this figure only, the ionization equilibria of Jordan (Table 2) were used. Note that in Figs. 7 and 8 the ordinates are wrongly labeled $G(T)$; they should have been labeled $G(T_e)$.

Examination of the $G(T_e)$ functions of these lines (Fig. 5) shows the corresponding temperature to be $T = 3.0 \times 10^6$ ° K. The relative insensitivity of this value to the observed line intensity ratio may be illustrated by noting that a 10 per cent change in the measured ratio corresponds to only a 3×10^4 ° K variation in the value of T, considerably less than the probable range of actual temperatures in the region.

A second method of deriving T compares the observed intensities of the O VIII Ly-α and Ly-β lines, the ratio of which should also be temperature-sensitive. The collision rates for this hydrogen-like ion have been given by Burgess (1961) and used by McWhirter and Hearn (1963), who give detailed values of the Gaunt factor and of the intensity ratio Ly-α to Ly-β for a range of temperatures. From their values, the present intensity ratio, Ly-α/Ly-β = 6.3, corresponds to an emission temperature of $T = 3.1 \times 10^6$ ° K. In this case, the line ratio is not very sensitive to T, and on this count alone the extremely close agreement with the value of T from the neon line comparison is probably fortuitous.

b) Active Region Size and the Abundance of Neon

The corresponding value of N_e^2V may now be obtained using the above value of T and the observed intensity of the oxygen lines, for which element the solar abundance appears reasonably well determined. Thus, for the O VIII Ly-α line, taking $A_z = 5.0 \times 10^{-4}$ (Pottasch 1967), and reading $G(T_e)$ from Figure 6

$$N_e^2V = \frac{130 \times 10^{-5} \times 10^4 \times 10^5 \times 10^{43}}{8 \times 0.3 \times 0.42 \times 1.6 \times 4.5} = 1.7 \times 10^{48} \text{ cm}^{-3}.$$

In principle, the abundance of any other element represented in the spectrum may now be obtained by use of equation (3) and the above values of T and N_e^2V. At the same time, the derived values should provide a commentary on the validity of the initial isothermal assumption. Thus, for neon, a comparison of the measured intensities of Ne IX 13.45 Å and O VIII 19 Å yields a value of the neon abundance of Ne:H = 5.5×10^{-5}. This value is not very dependent on the actual temperature model of the active region, because of the similarity in the $G(T_e)$–temperature relations for the Ne IX and O VIII lines. Thus, variation of the assumed temperature for the whole active region from 2.5×10^6 ° to 3.5×10^6 ° K modifies the computed abundance of neon over the range 6.7×10^{-5} to 3.4×10^{-5}. For comparison, the neon abundance obtained from an ultraviolet spectral line analysis (Pottasch 1964) is 7×10^{-5}, while the cosmic abundance given in Allen (1963) has the considerably higher value of 2.8×10^{-4}. Essentially it is the neon-to-oxygen abundance ratio that is determined from the present analysis, but taking an oxygen abundance of 6.8×10^{-4}, after Allen, *reduces* the neon abundances required by the X-ray data.

c) Analysis of the Iron and Nickel Lines and an Improved Active Region Model

The most notable fact of the observed Fe XVII spectrum, apart from its strength, is the serious disagreement between the relative line intensities and those predicted by the simple line-formation theory. This is evident from a comparison of the present measurement with the best available f-values, listed in Table 1, from which it is noted, in particular, that the $2p$–$3d$ to $2p$–$3s$ intensity ratio is considerably less than expected. A similar situation is found with the isoelectronic Ni XIX spectrum and may indicate considerable "mixing" of the closely adjacent excited levels in these complex ions. Also, a recent calculation by Bely (1967) has shown a large cross-section for the collisional excitation $2p \rightarrow 3p$ in Fe XVII, and it is estimated that this may result, via the allowed transition $3p \rightarrow 3s$, in a threefold increase in the population of the $3s$ level.

It is proposed, for the present analysis, to consider these line series in groups, comparing only the total intensity with the total f-values for all observed transitions from

levels with a common principal quantum number and taking effective f-values for the $2p$–$3s$ lines three times larger than in Table 1. When this is done, for Fe XVII, a comparison with the O VIII lines shows a strong dependence of the calculated iron abundance on the assumed value of T, reflecting now the difference in the temperature response of the emission functions of the Fe XVII and O VIII lines (Figs. 7 and 6). Thus, an isothermal model gives the following abundance of iron at different values of T:

	$T(10^6\ ^\circ\ \mathrm{K})$			
	3.0	3.5	4.0	5.0
Fe:H (10^{-5})	17	7.4	2.9	1.9

Because of the increasingly efficient production of Fe XVII at temperatures above $3 \times 10^6\ ^\circ$ K, particularly in relation to the corresponding production of O VIII, the iron abundance computed at $T = 3 \times 10^6\ ^\circ$ K will be an upper limit if any significant amount of active region material exists at a still higher temperature. Conversely, the high value of A_{Fe} found at $3 \times 10^6\ ^\circ$ K, compared with published values, may be an indication of the presence of hotter material in the present case. Further consideration of this point appears justified because of the current order-of-magnitude disparity between recently published solar abundances of the iron, silicon, and magnesium group of elements (e.g., Urey 1967) and the possibility of a check on the present active region model.

Fortunately, the simultaneous observation of lines of both Fe XVII and Fe XVIII allows a limit to be set on the amount of "extra-hot" material in the active region, independently of the iron abundance. This is apparent from Figure 7, where it is seen that the relative efficiency of producing Fe XVIII 14.25 Å to the Fe XVII lines increases very rapidly above $3 \times 10^6\ ^\circ$ K. Since only two lines of Fe XVIII are observed and these both correspond to the $2p$–$3d$ transition, it may be useful to compare their total intensity and f-value both with the $2p$–$3d$, $3s$ line group of Fe XVII and, separately, with the $2p$–$3d$ line group only of that ion. Thus, for the $2p$–$3d$ lines only, using f-values from Table 1 and $G(T_e)$ values from Figure 7, application of equation (3) gives a line group ratio at $3 \times 10^6\ ^\circ$ K of

$$\frac{\text{Fe XVII}}{\text{Fe XVIII}} = \frac{2.89 \times 8 \times 10^{-6}}{5.02 \times 1.5 \times 10^{-7}} = 31 .$$

The comparable measured ratio is 20. Similarly, for the $2p$–$3d$ and $2p$–$3s$ lines of Fe XVII, using the threefold $2p$–$3s$ f-values, the calculated line ratio is

$$\frac{\text{Fe XVII}}{\text{Fe XVIII}} = \frac{3.52 \times 1.0 \times 10^{-5}}{5.02 \times 1.5 \times 10^{-7}} = 47 ,$$

compared with the observed line ratio of 38.

Both comparisons reveal excess Fe XVIII emission, indicative of the presence of a quantity of material in the active region at a temperature above $3 \times 10^6\ ^\circ$ K. However, the total "extra-hot" material must be quite small. For a temperature of $4 \times 10^6\ ^\circ$ K, the additional quantity N_e^2V required to bring the above calculated and observed ratios into agreement is only 5–7 per cent of N_e^2V at $3 \times 10^6\ ^\circ$ K. If a still higher temperature were assumed to represent the extra-hot material, N_e^2V would be correspondingly smaller.

d) Abundance of Iron and Nickel in the Active Region

The addition of a hotter component to the 3×10^6 ° K active region model will preferentially add to the iron and nickel emission as compared with the emission in the O VIII and Ne IX lines. The calculated abundances of iron and nickel relative to oxygen will, as a result, be reduced. Thus, for the two-component active region model

$$N_e^2 V = 1.7 \times 10^{48} \text{ cm}^{-3} \text{ at } 3 \times 10^6 \text{ ° K},$$

$$N_e^2 V = 1.0 \times 10^{47} \text{ cm}^{-3} \text{ at } 4 \times 10^6 \text{ ° K},$$

the observed iron line emission requires an abundance Fe:H $= 1.4 \times 10^{-4}$. This remains slightly higher than the value of 9×10^{-5}, obtained by Pottasch (1967) from a revised analysis of solar ultraviolet spectra, incorporating dielectronic recombination, and very much greater than the photospheric value of 4×10^{-6} (Goldberg, Müller, and Aller 1964) derived from a study of the Fraunhofer absorption line spectrum.

A direct comparison of the nickel and iron isoelectronic line series may now be made to obtain the relative nickel abundance. Because of the possibility of a blend in the Ni XIX 13.77 Å line, the corresponding intensities and f-values of the $2p$–$3d$ lines of each ion are used. Thus, with the appropriate $G(T_e)$ values from Figure 7, the $3 + 4 \times 10^6$ ° K model gives an abundance ratio Fe:Ni = 6. In comparison, Pottasch (1967) has recently reported a value of 11 for the Fe:Ni ratio from his revised analysis of solar ultraviolet spectra, and Goldberg, Müller, and Aller (1960) found a ratio of 4.5 in the photosphere.

e) Coronal Disk Emission

From the profiles of individual lines it is evident that most of the O VII emission is derived from a broad source, probably from the whole visible corona, while the other lines all follow the solar longitude activity variations. It remains to check how complete this separation is and, in particular, to see what fraction of "disk emission" underlies the assumed "active region" components. For this purpose an estimate of the coronal disk emission may be obtained from the observed O VII line intensities. The relative intensities and $f[G(T)]$ values do show some excess strength in the higher energy lines; however, the differences are small and may be due to the neglect of recombination into higher levels (Dupree 1967). It appears likely that a good measure of the coronal disk emission parameters may be obtained from the O VII lines. Thus, for O VII 21.5 Å,

$$G(T)\, N_e^2 dV = \frac{3.6 \times 10^{-3} \times 10^4 \times 10^{43}}{8 \times 0.3 \times 0.69 \times 4.5} = 4.8 \times 10^{43}.$$

For a range of possible (isothermal) coronal disk temperatures:

	$T(10^6$ ° K)				
	1 0	1.2	1 4	1.6	1.8
$G(T)$ (10^{-6})	1 3	3 0	6 0	9 5	12
$N_e^2 V$ $(10^{49}$ cm$^{-3})$	3 7	1 6	0 8	0 5	0.4

In comparison, the solar minimum corona of van de Hulst (Allen 1963) gives a value of $N_e^2 V = 4.10^{49}$, while a consensus of studies of both ultraviolet and radio data indicates a coronal temperature of about 1.5×10^6 ° K. The determination of temperature is

probably the more reliable and, taking a value of 1.5×10^{6} ° K, a considerable disagreement is found between the presently observed O VII emission and that computed from the van de Hulst value of N_e^2V. It is possible that the observed line intensities are in error by a factor 2, since they lie at the low sensitivity, long-wavelength end of the crystal spectrometer. However, the earlier measurement of O VII by Blake *et al.* (1965) is in good agreement with the present result, and the O VII emission is not expected to exhibit marked solar cycle variations.

Taking the largest coronal values allowed by the present measurement, that is, $N_e^2V = 1.5 \times 10^{49}$ at $T = 1.5 \times 10^{6}$ ° K, we may now estimate the upper limits of coronal emission underlying the observed active region components of each "hotter" line. It is found that the active region model provides more than 90 per cent of the main component of each Ne IX and O VIII line and more than 99 per cent of the corresponding nickel and iron emission, consistent with the initial assumption of an active region source for these lines. In contrast, the computed emission of O VII from the 3×10^{6} ° K material is weak, being less than 20 per cent of the measured flux at 21.6 Å and in agreement with the observed broad profile of this line.

f) Continuum Emission

It was observed in § II that the continuum emission did not exceed one-fifth of the total line emission below 20 Å and one-fourth between 14.25 and 11 Å. Furthermore, no indication of the O IX recombination limit at 14.25 Å was apparent in the data. A calculation may be made, using the model parameters just obtained, to check the consistency of the active region model with this upper-limit continuum. Thus, for O IX, which may be expected to be the major source of recombination emission in the 11–14 Å band, the calculated recombination emission is of the order 4×10^{-5} erg cm^{-2} sec^{-1} Å^{-1}. Since at 3×10^{6} ° K the oxygen is already over 50 per cent fully ionized, the total continuum near 14 Å should not exceed 10^{-4} erg cm^{-2} sec^{-1} Å^{-1}, allowing both for an increase in the model temperature and for the contributions of other, less abundant, ions. Thus, it appears that the active region model derived from the observed line spectrum is also consistent with the non-observation of the solar X-ray continuum.

g) Comparison with Broad-Band Photographs

Some interesting comparisons may be drawn with recently published analyses of solar X-ray photographs in the 10–60 Å wave band, obtained with pinhole (Pounds and Russell 1966) and imaging reflector (Reidy *et al.* 1968) cameras. A study of some twenty active regions, from six sets of photographs, has shown a correspondence between the size (N_e^2V) of a coronal emission region and the area times intensity product of the associated plage, from which a predicted value of $N_e^2V = 2 \times 10^{48}$ cm^{-3} is obtained for combined plages 8278 and 8279, which formed the main northwest quadrant activity on May 5, 1966. This predicted value agrees well with the value found for the active region content from the present line spectrum.

The broad-band photographs also offer an interesting indication of the nature of the product N_e^2V. A typical coronal active region is found to have dimensions, on the disk, of about 1′, or 4.5×10^{4} km, and a similar extension in height. With these dimensions the present data give a mean electron density of 5×10^{9} cm^{-3} for the active region. This, again, is consistent with the X-ray photographs which show, typically, electron densities of from 3 to 8×10^{9} cm^{-3} for coronal regions associated with moderate plages.

The authors are indebted to Dr. C. Froese Fischer and to Drs. S. Kastner and J. H. Underwood for calculating several *f*-values used in this paper prior to publication. It is a pleasure also to acknowledge the provision of unpublished ionization equilibria by Dr. C. Jordan and by Dr. J. Allen and Mrs. A. K. Dupree.

REFERENCES

Allen, C. A. 1963, *Astrophysical Quantities* (2d ed.; London: Athlone Press).
Bely, O. 1967, *Solar Physics* (in press).
Blake, R. L. 1966, private communication.
Blake, R. L., Chubb, T. A., Friedman, H., and Unzicker, A. E. 1965, *Ap. J.*, **139**, 776.
Burgess, A. 1961, *Mém. Soc. Roy. Sci. Liège*, 5th ser., **4**, 299.
Charles, M. W., and Cooke, B. A. 1967, *J. Sci Instr.*, **44**, 976.
Culhane, J. L., Herring, J , Sanford, R., Phillips, R., and O'Shea, G 1966, *J. Sci. Instr.*, **43**, 908.
Dupree, A. K. 1967, private communication.
Evans, K , Pounds, K. A , and Culhane, J. L. 1967, *Nature*, **214**, 41.
Fritz, G., Kreplin, R. W., Meekins, J. F., Unzicker, A. E., and Friedman, H. 1967, *Ap J.* (*Letters*), **144**, L133.
Goldberg, L. 1964, *Abundance Determinations on Stellar Spectra* (London: Academic Press).
Goldberg, L., Müller, E. A , and Aller, L H. 1960, *Ap. J. Suppl.*, Vol. **5**.
James, R. W. 1948, *Optical Principles of the Diffraction of X-Rays* (London: Bell & Sons), p. 268.
Letfus, V. 1965, *Bull. Astr. Inst. Csl.*, **16**, 231.
McWhirter, R. W. P., and Hearn, A. G. 1963, *Proc. Phys. Soc.*, **82**, 641.
Pottasch, S. R. 1964, *Space Sci. Rev.*, **3**, 816.
———. 1966, *B.A.N.*, **18**, 237.
———. 1967, *ibid.*, **19**, 113.
Pounds, K. A., and Russell, P. C. 1966, *Space Research* (New York: Spartan Books), **6**, 34.
Reidy, W , Vaiana, G., Zehnpfennig, T , and Giacconi, R. 1968, *Ap. J.*, **151**, 333.
Rugge, H. R., and Walker, A. B. C. 1967, paper read at COSPAR, London, July, 1967.
Sawyer, G. A , Jahoda, F. C., Ribe, F. L., and Stratton, T. F. 1962, *J Quant. and Spectrosc Rad Transf.*, **2**, 467.
Underwood, J. A , and Stewardson, E. A. 1965, *Brit. J. Appl. Phys.*, **16**, 1877.
Urey, H. C. 1967, *Quart J R.A.S.*, **8**, 23